

Position Reconstruction in Scintillation Detectors

Borexino is one of a new generation of ultra-low-background scintillator-based detectors. Such detectors are widely used for the detection of weakly interacting particles. At present the main focus of observation is on neutrinos and antineutrinos from various sources, but there are also plans to construct large optical detectors to search for as yet undiscovered particles such as WIMPs. The detection mechanism is based on the collection of visible or ultraviolet photons. These are emitted as Čerenkov radiation (*e. g.*, as in Kamiokande [135] and SNO [136]) or as scintillation photons. This chapter will focus on a likelihood-based method of position reconstruction for scintillator-based, unsegmented detectors, and the spatial resolutions that may be expected from the method.

5.1 The need for spatial reconstruction

Due to the extremely low interaction rates of neutrinos and their antiparticles (to say nothing of WIMPs and so forth), it is necessary for a detector to contain a large mass of scintillator with very low levels of internal radioactive contamination [55]. Ultra-pure materials are also used in order to screen radioactivity from materials surrounding the

detector [55, 63]. Unfortunately, as already mentioned in Section 3.3, the photosensitive elements used to detect scintillation light are notorious for being among the main sources of radioactivity in an ultra-low-background detector.

It is therefore desirable to insert one or more layers of buffer material between the photosensitive elements and the scintillator to suppress radioactive background. Often the buffers are inactive, *i. e.*, not scintillating. An inactive buffer offers the advantage of minimizing the total trigger rate caused by the abundant radioactive decays generally produced within the photosensitive elements. Since the compositions of the scintillator and inactive buffer are different, a scintillator containment system analogous to the Borexino Inner Vessel is required to physically separate them. The containment system, being in direct contact with the scintillator, must satisfy stringent intrinsic radiopurity requirements.

For additional background prevention, the outer region of the scintillator volume can be used as an active buffer. This allows any residual radioactivity coming from the containment system, or passing through it, to be monitored and suppressed. A “fiducial volume” is commonly defined as a region at the center of the active volume of the detector in which radioactive background is expected to be at a minimum. The discrimination between events belonging to the fiducial and to the non-fiducial regions is performed by means of software implementation (reconstruction code) of an algorithm (reconstruction algorithm), which assigns to each single event a reconstructed position, either inside or outside the fiducial volume. The algorithm also provides a means of comparing the position of different events and is an important tool for the identification of several background sources. The designs of some planned detectors incorporate only a thin inactive buffer region or none at all, and in these cases, correct assignment of an event as belonging to the fiducial volume or the buffer region is even more important. The resolutions of detector reconstruction codes are generally studied with Monte Carlo methods. Event simulations allow close reproductions of the performance of these codes on real events. Typically, however, the reconstruction codes are fine tuned by calibrating the detector with the use of localized sources of radioactivity or light.

What seems lacking from the available literature is a comprehensive discussion of how the resolutions of detector reconstruction codes are related to some basic properties of the detector: the linear dimension, the time dispersion of the photon emission, the scintillator index of refraction, possible processes of absorption and re-emission and of scattering of the scintillator light, etc. Though some results are presented in [137], their form is complex due to the inclusion of various second-order effects such as light scattering and angular dependence of the photosensitive elements. This chapter presents an analytic study of the resolution for reconstruction in time and space of scintillation events. For simplicity, this study is restricted to the case of events at the center of the detector. Other analytical studies [137], full Monte Carlo simulations [80], and calibrations of existing experiments [138] show that the resolution of the reconstruction codes depends only mildly upon the location of the scintillation event.

This study also assumes that the optical properties of the media are uniform throughout the detector, that the indices of refraction of all materials between the active scintillator and the photodetectors are approximately the same, and that to a first approximation the scattering of light may be neglected.

5.2 Likelihood function derivation

The likelihood function is a standard statistical tool used to find parameters of a physical model. Suppose a set of N observations is composed of the independent values $\{t_i\}$ and dependent values $\{s_i\}$. For instance, $\{t_i\}$ could be a list of times at which a radioactive source is observed, and $\{s_i\}$ a list of observed activities at each time. We wish to model the data by some function $f(s)$ with n free parameters, represented by the n -vector \mathbf{a} . In the example, the function would be a decaying exponential, and the parameters would be the initial activity and the half-life. The likelihood function \mathcal{L} over the parameters is defined as a probability distribution for obtaining the observed data, given that the parameters \mathbf{a}

have the specific values \mathbf{a}_0 :

$$\mathcal{L}(\mathbf{a}_0; \{(t_i, s_i)\}) d^n s d^m t = \text{P}(\{(t_i, s_i)\} \text{ are observed} \mid \mathbf{a} = \mathbf{a}_0). \quad (5.1)$$

The infinitesimals on the left-hand side result from the definition of \mathcal{L} as a probability distribution function. The construct “ $\text{P}(A|B)$ ” is a standard way to abbreviate “the probability of condition A occurring, given that condition B is true.”

The difficult task is to calculate this probability based on the assumption that the data are correctly described by the model function $f(s)$. Once this has been done, in order to calculate the most probable value of the parameters of the model, one simply finds the maximum of the likelihood function (or, as is usually computationally easier, the minimum of $-\log \mathcal{L}$) in the n -dimensional space defined by the free parameters \mathbf{a} .

In the case of a scintillator-based detector, the parameters of interest are the position and time of an event in the detector, $\mathbf{a} = (\mathbf{x}_0, t_0)$. The observed data are the positions $\{\mathbf{x}_i\}$ of the photosensitive elements, usually PMTs (independent values), and the times $\{t_i\}$ at which each element detects a photon (dependent values); i ranges from 1 to N , with N being the number of detected photons. For now we assume that at most one photon is seen by each PMT, so all the \mathbf{x}_i 's are distinct, and N is also the number of PMTs that detect a photon. For conciseness, define the following possible conditions:

- A : an event occurs in the detector at position and time (\mathbf{x}_0, t_0)
- B : the positions and times at which PMTs detect photons are $\{(\mathbf{x}_i, t_i)\}$.

Then, Equation (5.1) becomes $\mathcal{L}(\mathbf{x}_0, t_0; \{(\mathbf{x}_i, t_i)\}) d^{3N} \mathbf{x} d^N t \equiv \text{P}(B|A)$.

5.2.1 Factoring the detector likelihood function

Let us assume that the times at which photons are emitted by the scintillator are uncorrelated. Then the likelihood function will have one independent factor for the piece of data

provided by each PMT.¹ Let the total number of working PMTs be T , so that N PMTs (labeled $1, \dots, N$) have detected a photon, and $T - N$ PMTs (labeled $N + 1, \dots, T$) have not. If we further define

- C_i : A photon arrives at PMT i at an unspecified time
- D_i : PMT i detects a photon (*i. e.*, converts it to a photoelectron)
- E_i : PMT i detects a photon at the specific time t_i ,

then

$$\begin{aligned} P(\mathbf{B}|\mathbf{A}) &= \prod_{i=1}^N P(E_i|\mathbf{A}, C_i, D_i) P(D_i|\mathbf{A}, C_i) P(C_i|\mathbf{A}) \\ &\times \prod_{j=N+1}^T [P(\neg D_j|\mathbf{A}, C_j) P(C_j|\mathbf{A}) + P(\neg C_j|\mathbf{A})] \end{aligned} \quad (5.2)$$

(where \neg is the logical negation symbol). Of course, $P(D_i|\mathbf{A}, C_i)$ is just the total efficiency q_i of PMT i , which for simplicity will be supposed independent of the original event position. This assumption is reasonable if, for instance, the PMTs are mounted at a distance from the fiducial volume of the detector, so arriving photons always have a small angle of incidence.

Now define a “per-PMT” likelihood function \mathcal{L}_i (we absorb the infinitesimals into the function definition for later convenience),

$$\mathcal{L}_i(\mathbf{x}_0, t_0; \mathbf{x}_i, t_i) = \begin{cases} q_i P(E_i|\mathbf{A}, C_i, D_i) P(C_i|\mathbf{A}), & i \leq N \\ (1 - q_i) P(C_i|\mathbf{A}) + P(\neg C_i|\mathbf{A}), & N < i \leq T. \end{cases} \quad (5.3)$$

¹Strictly speaking, this is not precisely true. We assume in this discussion that exactly N PMTs detected photons, instead of making the more basic assumption that exactly Γ scintillation photons were emitted, which would lead to the number of PMTs that see photons having a Poissonian distribution with some mean value $\bar{N}(\Gamma)$. With our assumption of N photons detected, the PMT hit data are in fact weakly correlated. For N reasonably large, though, the difference when $N = \bar{N}$ should be negligible. It would be interesting to compare results derived from the often-used Poisson and multinomial probabilistic models to the model put forth here.

The total likelihood function (times infinitesimals) is then the product of all per-PMT likelihood functions. Notice that the per-PMT likelihood function of a supposedly dead PMT ($q_i = 0$) that does not detect a photon reduces to 1, so does not influence the total likelihood function, just as expected.

5.2.2 Scintillator dispersion time at the emission point

The first non-trivial factor in the expression for the likelihood function of a PMT that detects a photon is based solely on timing information of a photon emitted by the scintillator. Scintillation photons are emitted, as discussed in Section 3.1, as a consequence of the ionization of the scintillator due to interacting particles or radioactive decays. The typical dispersion in the time of emission of organic liquid scintillators is on the order of a few nanoseconds, with a slower component that can reach hundreds of nanoseconds. Since electronically excited scintillator molecules retain no memory of the original direction of the ionizing particle, their emission of photons is isotropic. In this discussion we also assume that the time of emission of each photon, relative to the time of the event causing scintillation, is an independent random variable τ_e with probability density function $p(\tau_e)$.

We also refer to the function $p(\tau_e)$ as the scintillator response function. Its experimental determination will be described a bit in Section 7.5; in this chapter we take it as a given. Referring to the left half of Figure 5.1, one sees that at a specific time t , this function may also be regarded as an outgoing spherical photon probability wave, integrated over the solid angle 4π . In fact, the most important factor in Equation (5.2), the probability $P(E_i|A, C_i, D_i)$, is equal to it. Let τ_f^i be the time of flight from the origin \mathbf{x}_0 of the photon to the position \mathbf{x}_i of the i^{th} PMT. Then, with n being the scintillator index of refraction, we have:

$$\tau_f^i = \frac{|\mathbf{x}_i - \mathbf{x}_0| n}{c} \quad (5.4)$$

$$t_i = \tau_e + \tau_f^i + t_0. \quad (5.5)$$

As a result,

$$\mathcal{L}_i(\mathbf{x}_0, t_0; \mathbf{x}_i, t_i) \propto p(t_i - t_0 - \tau_f^i). \quad (5.6)$$

Of course, factors other than the dispersion time of the scintillator may also affect the probability distribution function of the recorded arrival times of photons at PMTs. The most important other effects are usually the effects of scattering and absorption and re-emission processes in the scintillator, as well as the finite time resolution of the PMTs themselves. The latter may in general be incorporated into the distribution $p(\tau_e)$ by convolution with the scintillator dispersion function. The former require a bit more care because scattering effects depend in general upon the light path length from the event to the PMT; a full treatment of these effects is beyond the scope of this chapter. Some description of them may be found in, for instance, references [75, 80].

5.2.3 Photon attenuation

As photons travel away from their origin, they are attenuated by the familiar inverse square law. This implies a formula for the probability $P(C_i|A)$ that a given PMT is hit by a scintillation photon. Suppose a PMT of infinitesimal area, at a distance $s_i \equiv |\mathbf{x}_i - \mathbf{x}_0|$ from the event, subtends a solid angle $d\Omega_i$ as seen from the event location. It will be struck by only a fraction $d\Omega_i/4\pi$ of all photons emitted. So if Γ photons were emitted, its probability of being hit by at least one of them is

$$P(C_i|A) = 1 - \left(1 - \frac{d\Omega_i}{4\pi}\right)^\Gamma \approx \Gamma \frac{d\Omega_i}{4\pi}. \quad (5.7)$$

If the i^{th} PMT has an area dA_i and is tilted away from the line of sight by an angle ψ_i , as shown on the right half of Figure 5.1, then $d\Omega_i = \cos \psi_i dA_i/s_i^2$, so the resulting factor in the likelihood function is given by

$$\mathcal{L}_i(\mathbf{x}_0, t_0; \mathbf{x}_i, t_i) \propto \Gamma \frac{d\Omega_i}{4\pi} = \Gamma \frac{\cos \psi_i}{4\pi s_i^2} dA_i. \quad (5.8)$$

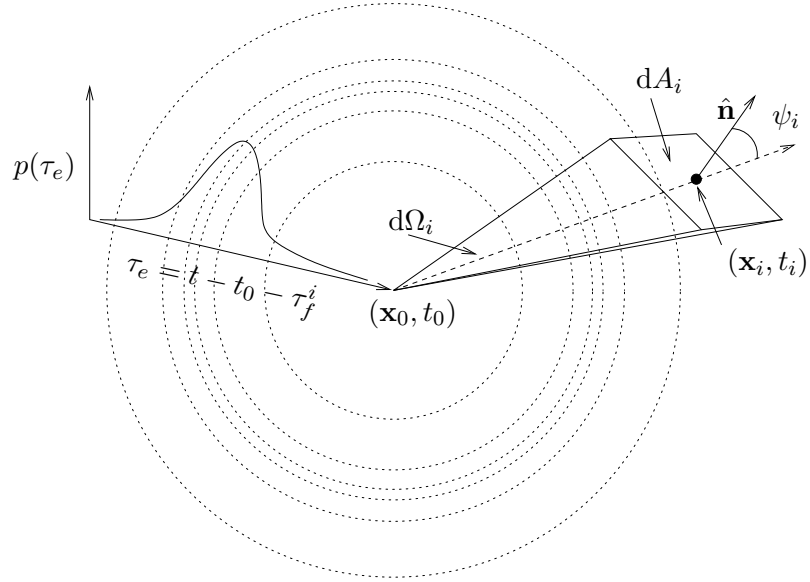


Figure 5.1: Geometry of the likelihood function derivation. The concentric dotted lines, and the graph on the left, represent the probability function (an expanding spherical wave) of the emission time of a scintillation photon. The rectangle labeled dA_i represents a PMT of infinitesimal size with normal vector $\hat{\mathbf{n}}$, subtending a solid angle $d\Omega_i$ as seen from the position of the detector event. The PMT is tilted away from the direction of the event by an angle ψ_i . Note that we have not yet made any assumptions about the geometry of the detector.

As mentioned already, all constant factors in a likelihood function may be discarded with no effect on the location in parameter space of its maximum. To first order, this includes the efficiency q_i of each PMT. The per-PMT likelihood function for a PMT detecting a photon may thus be redefined as

$$\mathcal{L}_i(\mathbf{x}_0, t_0; \mathbf{x}_i, t_i) = p(t_i - t_0 - \tau_f^i) \frac{\cos \psi_i}{s_i^2}. \quad (5.9)$$

Its logarithm is

$$\log \mathcal{L}_i = \log p(t_i - t_0 - \tau_f^i) + \log \cos \psi_i - 2 \log s_i. \quad (5.10)$$

5.2.4 The PMTs not triggered

For completeness, we now consider the case of a PMT that does not detect a photon produced by an event in the detector. Its per-PMT likelihood function, from Equation (5.3), is given by

$$\begin{aligned}
 \mathcal{L}_i(\mathbf{x}_0, t_0) &= (1 - q_i)P(C_i|A) + P(-C_i|A) \\
 &= (1 - q_i) \left[1 - \left(1 - \frac{d\Omega_i}{4\pi} \right)^\Gamma \right] + \left(1 - \frac{d\Omega_i}{4\pi} \right)^\Gamma \\
 &= 1 - q_i + q_i \left(1 - \frac{d\Omega_i}{4\pi} \right)^\Gamma \\
 &\approx 1 - q_i \Gamma \frac{d\Omega_i}{4\pi}.
 \end{aligned} \tag{5.11}$$

The logarithm of this per-PMT likelihood function is $\approx -q_i \Gamma d\Omega_i / 4\pi$. This term, containing an infinitesimal, is negligible in size compared to the terms of Equation (5.10) coming from per-PMT likelihood functions for PMTs that have detected a photon. If PMTs are in fact very small compared to any other relevant dimensions of the detector, it may therefore be ignored.

5.2.5 Specialization to a spherical detector

As written, Equation (5.9) is applicable to any detector with pointlike PMTs forming the vertices of a convex polyhedron (so that light from an event at any point inside the detector may reach any one of the PMTs). Let us specialize to a spherical detector centered at the origin, having a uniform distribution of inward-facing PMTs at distance R from the detector center. The radius of the fiducial volume of the detector itself may be less than R ; it is not an important quantity for this discussion. As above, we call the distance from an event to the i^{th} PMT $s_i \equiv |\mathbf{x}_i - \mathbf{x}_0|$. Let the distance from the center of the detector to the event be $a \equiv |\mathbf{x}_0|$, so we have the geometry of Figure 5.2.

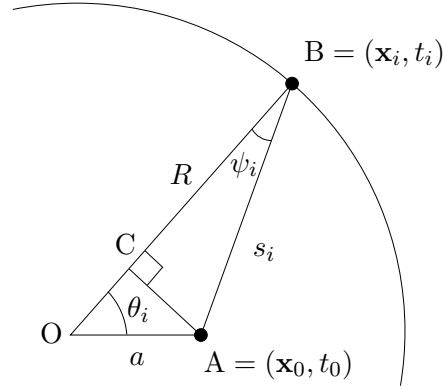


Figure 5.2: Geometry of a spherical detector.

By dropping a perpendicular from point A to segment OB at point C, one readily sees that $s_i \cos \psi_i = R - a \cos \theta_i$, with θ_i being the angle between the event and the i^{th} PMT as seen from the origin. Hence the likelihood function becomes

$$\mathcal{L}(\mathbf{x}_0, t_0; \{(\mathbf{x}_i, t_i)\}) = \prod_{i=1}^N p\left(t_i - t_0 - \frac{s_i n}{c}\right) \frac{R - a \cos \theta_i}{s_i^3} \quad (5.12)$$

where s_i is given by the Law of Cosines,

$$s_i^2 = R^2 + a^2 - 2aR \cos \theta_i. \quad (5.13)$$

5.3 Analytical treatment of the likelihood function

It may be of interest to examine properties of the likelihood function in the particular case of a hypothetical event occurring at the center of a spherical detector. This allows the general nature of the problem of reconstruction to be understood analytically. For simplicity, let's assume that the distribution of the time emission of the photons is a Gaussian curve with width equal to the characteristic dispersion time of the scintillator:

$$p(\tau_e) = \frac{e^{-\tau_e^2/2\sigma^2}}{\sqrt{2\pi\sigma^2}}; \quad \log p(\tau_e) = \text{const} - \frac{\tau_e^2}{2\sigma^2}. \quad (5.14)$$

The same equation can also be used for the case when the original scintillation light is absorbed and then re-emitted by scintillation fluors in the immediate proximity of the energy deposition point, as with PPO in pseudocumene. In this case, the dispersion characteristic of the scintillator is effectively broadened by the absorption and re-emission process.

5.3.1 Taylor expansion of the likelihood function

For a point in the detector at a distance a from the center, in the direction of a particular unit vector $\hat{\mathbf{u}}$, the log likelihood function is

$$\log \mathcal{L}(a\hat{\mathbf{u}}, t_0) = \text{const} - \frac{1}{2\sigma^2} \sum_{i=1}^N \left(t_i - t_0 - \frac{s_i n}{c} \right)^2 + \sum_{i=1}^N \log \frac{R - a \cos \theta_i}{s_i^3} \quad (5.15)$$

where s_i and θ_i for each PMT are as shown in figure 5.2. We assume that the number of hit PMTs N is sufficiently large that we can, with little error, replace this expression by spatial and temporal averages over the expected angular and time distributions of the PMT hits. That is (discarding the constant term),

$$\log \mathcal{L}(a\hat{\mathbf{u}}, t_0) \approx -\frac{N}{2\sigma^2} \left\langle \left(t - t_0 - \frac{sn}{c} \right)^2 \right\rangle + N \left\langle \log \frac{R - a \cos \theta}{s^3} \right\rangle, \quad (5.16)$$

where t , s , θ are now continuous random variables with the expected distributions. We now calculate these averages for a point-like event located in the center $\mathbf{x}_0 = \mathbf{0}$ of the detector, occurring at time $t_0 = 0$.

First consider the time average. The time of flight of photons from the center to each PMT (assuming minimal scattering) is Rn/c , where n is the index of refraction and c is the velocity of light in vacuum. This means that the distribution curve of t is $p(t - Rn/c)$. From the properties of a Gaussian distribution, the time averages of time-dependent quantities are

$$\langle t \rangle = \frac{Rn}{c} \quad (5.17)$$

$$\langle t^2 \rangle = \langle t \rangle^2 + \sigma_t^2 = \frac{R^2 n^2}{c^2} + \sigma^2. \quad (5.18)$$

Likewise, since all PMTs are equidistant from an event at the center of a spherical detector, the distribution of PMT hits should be uniform over the solid angle. Hence the spatial averages over quantities dependent upon the event-to-PMT angle θ can be found using Equation (5.13) and taking the surface integral over the sphere of PMTs:

$$\langle s \rangle = \frac{1}{4\pi} \int d\phi d(\cos \theta) \sqrt{R^2 + a^2 - 2aR \cos \theta} = R + \frac{a^2}{3R} \quad (5.19)$$

$$\langle s^2 \rangle = \frac{1}{4\pi} \int d\phi d(\cos \theta) (R^2 + a^2 - 2aR \cos \theta) = R^2 + a^2 \quad (5.20)$$

Finally, we observe that for a point-like event in the center of a uniform sphere of PMTs, there is no correlation between the expected spatial distribution of s and temporal distribution of t ; that is, $\langle st \rangle = \langle s \rangle \langle t \rangle$. This and the above equations allow us to evaluate

$$\begin{aligned} \left\langle \left(t - t_0 - \frac{sn}{c} \right)^2 \right\rangle &= \left\langle t^2 + t_0^2 + \frac{s^2 n^2}{c^2} - 2tt_0 - 2t \frac{sn}{c} + 2t_0 \frac{sn}{c} \right\rangle \\ &= \frac{R^2 n^2}{c^2} + t_0^2 + (R^2 + a^2) \frac{n^2}{c^2} - 2 \frac{Rn}{c} t_0 \\ &\quad - 2 \frac{Rn^2}{c^2} \left(R + \frac{a^2}{3R} \right) + 2t_0 \left(R + \frac{a^2}{3R} \right) \frac{n}{c} \\ &= \text{const} + t_0^2 + \frac{n^2}{3c^2} a^2 + \frac{2n}{3cR} a^2 t_0 \end{aligned} \quad (5.21)$$

where the constant term contains whatever does not depend explicitly on t_0 and a .

The quantity averaged over in the last term of Equation (5.16), again substituting in Equation (5.13), becomes

$$\begin{aligned} \log \frac{R - a \cos \theta_i}{s_i^3} &= \log \left(\frac{R - a \cos \theta_i}{(R^2 + a^2 - 2aR \cos \theta_i)^{3/2}} \right) \\ &= -2 \log R + \frac{2a}{R} \cos \theta_i + \frac{a^2}{2R^2} (5 \cos^2 \theta_i - 3) + \dots \end{aligned} \quad (5.22)$$

with the last equality above being the expansion into a Taylor series in a/R .

By once again averaging the expected distributions in s and θ over the solid angle, the result, obtained to second order in a/R , is determined to be

$$\left\langle \log \frac{R - a \cos \theta}{s^3} \right\rangle \approx \text{const} - \frac{2a^2}{3R^2}. \quad (5.23)$$

The complete likelihood function for an event at the center of a spherical detector, to second order in a/R , is thus

$$\log \mathcal{L}(a\hat{\mathbf{u}}, t_0) \approx \text{const} - N \left[\frac{1}{2\sigma^2} \left(t_0^2 + \frac{n^2}{3c^2} a^2 + \frac{2n}{3cR} a^2 t_0 \right) + \frac{2}{3R^2} a^2 \right]. \quad (5.24)$$

5.3.2 Likelihood function maximum and resolutions

Solving for the maximum of the likelihood function and requiring $|a| < R$ gives the expected solutions:

$$\begin{cases} \frac{\partial}{\partial t_0} \log \mathcal{L} = 0 \\ \frac{\partial}{\partial a} \log \mathcal{L} = 0 \end{cases} \iff \begin{cases} t_0 = 0 \\ a = 0 \end{cases} \quad (5.25)$$

We next ask about the expected resolution of the detector. Notice that the information matrix is diagonal because the off-diagonal terms, $-\partial^2(\log \mathcal{L})/\partial a \partial t_0$, are zero when $a = t_0 = 0$. The theoretical resolutions of the detector in space and time are therefore given by reciprocals of the second derivatives of the likelihood function:

$$\begin{cases} \delta t_0 = \left(-\frac{\partial^2 \log \mathcal{L}}{\partial t_0^2} \right)^{-1/2} = \frac{\sigma}{\sqrt{N}} \\ \delta a = \left(-\frac{\partial^2 \log \mathcal{L}}{\partial a^2} \right)^{-1/2} = \left(\frac{Nn^2}{3c^2\sigma^2} + \frac{4N}{3R^2} \right)^{-1/2} \end{cases} \quad (5.26)$$

When the detector dimensions are much larger than the scintillator dispersion time, $R \gg c\sigma/n$, we can approximate $\delta a \approx \sqrt{\frac{3}{N}} \frac{c\sigma}{n}$. (It should be noted that this does not take into account scattering effects, which become increasingly important with larger detectors.) After the appropriate simplifications, this is in good agreement with Equation (64) of reference [137].

Because of the spherical symmetry of the problem, δa can be used as a stand-in for any of the three Cartesian spatial resolutions δx_0 , δy_0 , δz_0 . One may, for instance, make the

substitution $a^2 = x_0^2 + y_0^2 + z_0^2$ in Equation (5.24) and obtain the same results for the resolution in each Cartesian coordinate.

5.3.3 Pattern matching

In case of use of a liquified noble gas as scintillator, as in the new generation of solar neutrino detectors [139, 140], Rayleigh scattering of the ultraviolet scintillation photons plays an important role. The photons are scattered intensely by the medium, such that they effectively diffuse out of the medium with a very long dispersion time; then $R \gg c\sigma/n$ is no longer valid. In this case, the information carried by the time of flight method about the original position of the events becomes less reliable. However, it is still possible to reconstruct the original position of the event by taking into account that the density of hits on the PMTs decreases with the inverse of the squared distance from the point where the energy is deposited [141].

Suppose that we have no timing information, so our only information about an event is the pattern of hit PMTs. In this case, the likelihood function simply determines the position of the event. It does not depend on time and cannot be used to reconstruct the time itself. We may set the function $p(\tau_e)$ to be constant and ignore it:

$$\log \mathcal{L}(a\hat{\mathbf{u}}) = \text{const} + \sum_{i=1}^N \log \frac{R - a \cos \theta_i}{s_i^3}. \quad (5.27)$$

By the same methods as above, we obtain

$$\log \mathcal{L}(a\hat{\mathbf{u}}) \approx \text{const} - \frac{2N}{3R^2} a^2 \quad (5.28)$$

for the second-order Taylor expansion in a/R of the likelihood function for an event at the detector center. In this case we find

$$\frac{\partial}{\partial a} \log \mathcal{L} = 0 \iff a = 0, \quad (5.29)$$

Detector	R [m]	T	n	σ [ns]	ϵ [pe]	N	Pred. δa [cm]	Obs.
Organic scintillator detectors								
CTF, ^{214}Po α [138, 143]	3.3	100	1.8	5.1	225	90	12.0	12.3
Borexino, 1 MeV e^- MC [55]	6.5	2240	1.5	5.1	400	366	8.8	8.0
Hypothetical ℓNe detector, 100 keV e^- MC [142]								
Spatial data only	3.0	1832	-	-	243	243	16.7	17.0
Timing included	"	"	1.2	10	162	155	15.0	13.6

Table 5.1: Comparison of the predicted resolutions of three liquid scintillator detectors with the values determined experimentally or by Monte Carlo (MC) methods. See the text for meanings of the columns and comments on values in *italics*.

and for the resolution,

$$\delta a = \left(-\frac{\partial^2 \log \mathcal{L}}{\partial a^2} \right)^{-1/2} = \sqrt{\frac{3}{N}} \frac{R}{2}. \quad (5.30)$$

Recall Equations (5.24) and (5.26) in the case where timing information *is* available:

$$\begin{aligned} \log \mathcal{L}(a\hat{\mathbf{u}}, t_0) &\approx \text{const} - \frac{2N}{3R^2} a^2 - \frac{N}{\sigma^2} \left(t_0^2 + \frac{n^2}{3c^2} a^2 + \frac{2n}{3cR} a^2 t_0 \right) \\ \delta a &= \left(\frac{Nn^2}{3c^2\sigma^2} + \frac{4N}{3R^2} \right)^{-1/2} \approx \sqrt{\frac{3}{N}} \frac{c\sigma}{n}. \end{aligned}$$

We see that use of timing information improves spatial resolution significantly when the scintillator dispersion time is much less than the travel time for light to cross the detector. In a liquid noble gas detector, the scintillator time dispersion is very broad due to the amount of internal Rayleigh scattering of scintillation light. Nevertheless, use of even the small amount of timing information available has been shown to improve the spatial resolution by a large fraction [142].

5.3.4 Comparison to observed resolutions

Experimentally, the position resolution of a detector can be determined in several ways. The simplest and most common is the use of a calibration source. In cases when the detector

has not yet been built, Monte Carlo methods are of course the only method that can be used. The detector resolutions obtained from experimental results for the Counting Test Facility (the Borexino 4-ton prototype), and from Monte Carlo simulations of Borexino and a hypothetical liquid neon dark matter detector [142], are shown in the last column of Table 5.1. For comparison, the physical attributes of the detectors and the predicted resolutions δa from Equation (5.26) are shown in the other columns of the table. As above, R is the detector radius, T the total number of PMTs, n the scintillator index of refraction, and σ the scintillator dispersion time. The average number of photoelectrons detected in each event from the source used is denoted by ϵ .

N is determined in most cases as follows. In detectors using a time-of-flight position reconstruction method, each PMT can measure the arrival time only of the first photon it detects. This difficulty will be discussed more thoroughly in Section 5.4. The immediate consequence is that N is a measure of the number of hit PMTs rather than the total number of detected photoelectrons. Basic probability tells us that given an event in which ϵ photoelectrons are detected, the expected number of hit PMTs is

$$\langle N \rangle = T \left[1 - \left(\frac{T-1}{T} \right)^\epsilon \right]. \quad (5.31)$$

Note, however, that for the spatial hit pattern, every photoelectron contributes to our knowledge, even for multiple hits on a single PMT. This implies that the term $4N/3R^2$ in the expression for δa in Equation (5.26) should in fact include ϵ , not N . In calculating the predicted values of δa in Table 5.1, we therefore use the modified expression

$$\delta a = \left(\frac{Nn^2}{3c^2\sigma^2} + \frac{4\epsilon}{3R^2} \right)^{-1/2}. \quad (5.32)$$

Some comments on idiosyncracies of the individual detectors are in order. The data used for the Counting Test Facility (CTF) are from the set of measurements taken by its first incarnation, known as CTF 1 (see Section 6.4.1). The value $n = 1.8$ tabulated for CTF 1 is an “effective index of refraction.” The software historically used to analyze events in the CTF detector does not take into account the possibility of more than one photon detected

per PMT; as will be explained in Section 7.1.1, the value of n used in the reconstruction must be increased in order to balance this effect. Additionally, note that the observed value of δa for the CTF takes into account only the spread in x and y coordinates; the CTF source had the shape of a cylinder, extended in z .

In the hypothetical liquid neon detector described in reference [142], events have a prompt component (relative intensity 2.0) and a delayed component (relative intensity 1.0) of scintillation light. For the Monte Carlo simulation taking into account only the spatial pattern of PMT hits (“spatial data only” row of Table 5.1), both components contribute useful data. In that case the photoelectron yield is 2428 pe/MeV, 1.5 times the prompt light yield of 1619 pe/MeV (10791.7 photons/MeV \times 20% quantum efficiency \times 75% geometric coverage) quoted in the reference. For the position reconstruction calculated from the spatial pattern only, we use $N = \epsilon_{total} \equiv \epsilon_{prompt} + \epsilon_{delayed}$ in Equation (5.30).

Calculation of the expected resolution in the liquid Ne detector is trickier when timing information is included (“timing included” row of table 5.1). The two terms contributing to δa in Equation (5.32) must be evaluated with different values for ϵ . The term $4\epsilon/3R^2$ comes from the spatial hit pattern and so uses $\epsilon_{total} = 243$, while the timing-dependent term $Nn^2/3c^2\sigma^2$ includes only the prompt component of scintillation light, and thus uses $\epsilon_{prompt} = 162$, with $N = 155$ derived from Equation (5.31).

The source of the largest potential errors in the predictions of Table 5.1 is the value of the scintillator dispersion, σ . The true scintillator dispersion function of a detector $p(\tau_e)$ is not actually a Gaussian, so the use of Equation (5.26) is only an approximation. The value of 5.1 ns used for σ in the CTF is obtained from the fit to a CTF 1 scintillator response function described in reference [80]. The parameters of this fit, shown in Figure 7.3, are given in Section 7.5; the function was sampled at 1 ns intervals and fit to a pure Gaussian in order to obtain a value for σ . (The same scintillator dispersion function was used in the Borexino Monte Carlo simulations.) Nevertheless, the predicted, observed and Monte Carlo values of the position resolution are in quite good agreement. For the liquid Ne detector,

σ was estimated at 10 ns, based on Figure 7 of reference [142], as $\frac{1}{2}$ the difference between times with probability values equal to $e^{-1/2}$ times the value at the peak. One could plausibly estimate this value of σ to be anywhere in the range 5.5 to 15 ns, yielding estimates of δa from 12.6 to 15.9 cm. This range brackets the Monte Carlo simulation nicely.

5.4 Multiple PMT occupancy

So far it has largely been assumed that the occupancy of each PMT in the detector is at most one. If the detector has the capability to measure the time at which *every* detected photon hits a given PMT, or if the detector (as with some of the proposed noble gas detectors) has no timing capability at all, then the assumption may be lifted with no effect, except that some of the \mathbf{x}_i (and hence θ_i and s_i) will be identical in Equation (5.12). For a detector with timing capabilities, however, it is more likely that the detector only has the capability to measure the arrival time of the *first* photon detected by each PMT. The probability function of the first detected photon to reach a PMT is not the same as that of a random photon detected by the same PMT; it is biased toward earlier times. To account for this bias, the scintillator response function $p(\tau_e)$ must be corrected.

5.4.1 Correcting for timing bias

Let the probability function of the first photon detected by a PMT, out of the n photons seen by that PMT from an event, be represented by $p_n(\tau_e)$. (Naturally, $p_1(\tau_e) \equiv p(\tau_e)$ by definition.) This is known as the “first order statistic.” In general, the corrected scintillator response function p_{corr} would then be some linear combination of the first order statistics,

$$p_{corr}(\tau_e) = \sum_{n=1}^{\infty} p_n(\tau_e) \times P(n \text{ photons hit the PMT}), \quad (5.33)$$

and an *a priori* guess would have to be made for the probability that each possible number of photons was seen by the PMT. For simplicity, let us assume that the number of photons

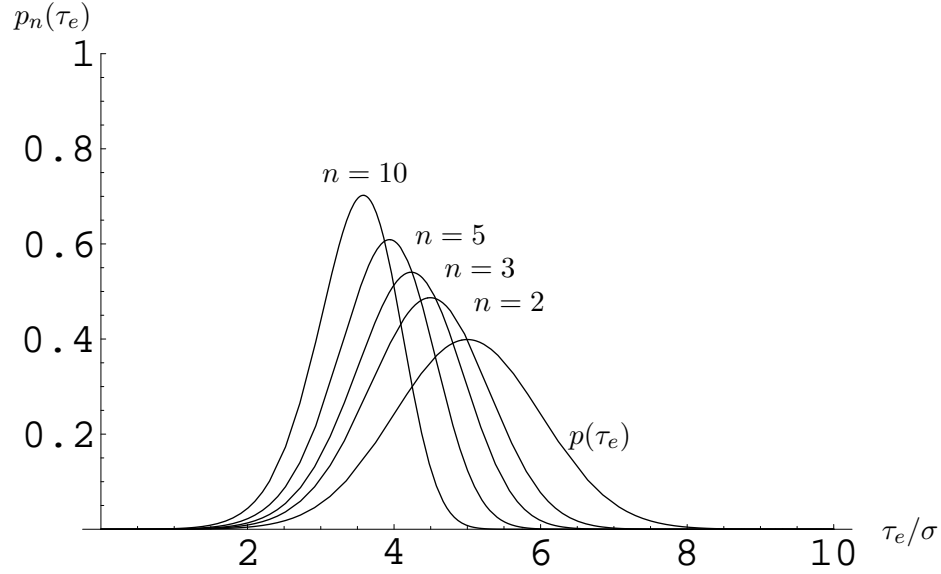


Figure 5.3: A hypothetical Gaussian scintillator response functions $p(\tau_e)$ and its first order statistics for increasing values of $n = 2, 3, 5, 10$. Note how as n increases, the corrected response function narrows and shifts toward earlier times. The time axis is shown in units of the scintillator dispersion time σ .

detected by each PMT for an event is known (in Borexino, for instance, this is determined via ADC channels separate from the timing channels). We can then set p_{corr} equal to the function $p_n(\tau_e)$.

It remains only to calculate $p_n(\tau_e)$ given $p(\tau_e)$ and n . Label the emission times of the n photons detected by a given PMT in some random order unrelated to timing (for instance, in order of increasing photon energy or increasing z component of momentum) as τ_1, \dots, τ_n . Also number them in order of increasing emission time as s_1, \dots, s_n . Then $p_n(\tau_e)$ is the probability function of the randomly chosen emission time τ_1 given that $s_1 = \tau_1$:

$$\begin{aligned}
 p_n(\tau_e) d\tau_e &= \text{P}(\tau_1 \in [\tau, \tau + d\tau] | \tau_1 = s_1) \\
 &= \text{P}(\tau_1 = s_1 | \tau_1 \in [\tau, \tau + d\tau]) \times \frac{\text{P}(\tau_1 \in [\tau, \tau + d\tau])}{\text{P}(\tau_1 = s_1)} \\
 &= \frac{p(\tau_e) d\tau_e}{(1/n)} \text{P}(\tau_1 = s_1 | \tau_1 \in [\tau, \tau + d\tau]),
 \end{aligned} \tag{5.34}$$

where the second equality is once again due to Bayes' Theorem. The probability in the last line above is just the probability that every other detected photon has a later arrival time than the randomly selected value τ_1 :

$$\begin{aligned}
 \text{P}(\tau_1 = s_1 | \tau_1 \in [\tau, \tau + d\tau]) &= \prod_{i=2}^n \text{P}(\tau_i > \tau_1 | \tau_1 \in [\tau, \tau + d\tau]) \\
 &= \text{P}(\tau_2 > \tau_1 | \tau_1 \in [\tau, \tau + d\tau])^{n-1} \\
 &= \left[\int_{\tau_e}^{\infty} p(\tau'_e) d\tau'_e \right]^{n-1}.
 \end{aligned} \tag{5.35}$$

Hence (letting $F(\tau_e) \equiv \int_{-\infty}^{\tau_e} p(\tau'_e) d\tau'_e$ represent the cumulative distribution function of τ_e), the first order statistic of $p(\tau_e)$, if n photons are detected by a given PMT, is

$$p_n(\tau_e) = np(\tau_e) [1 - F(\tau_e)]^{n-1}. \tag{5.36}$$

(This equation is derived independently in, for example, reference [144].)

Graphs of the first order statistics of a representative scintillator response function are shown in Figure 5.3 for values of n equal to 1, 2, 3, 5, and 10. (The specific response function shown is a Gaussian, Equation (5.14) offset by five units of σ from time zero.) Note how as n increases, the time distribution of the first PMT hit narrows and shifts toward earlier times.

5.4.2 Effects on detector resolution

One may ask about the effect of this correction on the likelihood function and spatial resolution. Consider again the case of a Gaussian scintillator time response function. We have

$$\log p_n(\tau_e) = \text{const} + \log p(\tau_e) + (n - 1) \log[1 - F(\tau_e)]. \tag{5.37}$$

Substituting in $F(\tau_e) = \frac{1}{2}[1 + \text{erf}(\tau_e/\sigma\sqrt{2})]$, the Taylor expansion to second order in τ_e becomes

$$\log p_n(\tau_e) = \text{const} - (n-1)\sqrt{\frac{2}{\pi}}\frac{\tau_e}{\sigma} - \left(\frac{1}{2} + \frac{n-1}{\pi}\right)\frac{\tau_e^2}{\sigma^2} + O(\tau_e^3). \quad (5.38)$$

That is, the first photon detected by each PMT contributes to the log of the likelihood function in the amount of $-\tau_e^2/2\sigma^2$, but each additional photon seen contributes only in the amount of $-\tau_e^2/\pi\sigma^2$ (plus a term linear in τ_e which has relatively little effect on the resolution for a large detector); compare to Equation (5.14). The resolution is better than if the corrected scintillator response function were not used, but still poorer than if the time of arrival of every detected photon were known.

Suppose that the total number of photons detected is ϵ , by N PMTs, and in particular that the i^{th} PMT sees n_i photons. Denoting the emission time by $\tau_e^i \equiv t_i - t_0 - s_i n/c$, the general likelihood function is then

$$\begin{aligned} \log \mathcal{L}(a\hat{\mathbf{u}}, t_0) &= \text{const} - \frac{1}{\sigma^2} \sum_{i=1}^N \left(\frac{1}{2} + \frac{n_i - 1}{\pi}\right) (\tau_e^i)^2 \\ &\quad - \frac{1}{\sigma} \sqrt{\frac{2}{\pi}} \sum_{i=1}^N (n_i - 1) \tau_e^i + \sum_{j=1}^{\epsilon} \log \frac{R - a \cos \theta_j}{s_j^3}. \end{aligned} \quad (5.39)$$

Define the excess photoelectron multiplicity as $\delta \equiv (\epsilon - N)/N$. The likelihood function in the limit of homogeneous PMT coverage as $N \rightarrow \infty$, for an event at the detector center, becomes

$$\begin{aligned} \log \mathcal{L}(a\hat{\mathbf{u}}, t_0) &= \text{const} - \frac{N}{\sigma^2} \left(\frac{1}{2} + \frac{\delta}{\pi}\right) \langle (\tau_e^i)^2 \rangle \\ &\quad - \frac{N\delta}{\sigma} \sqrt{\frac{2}{\pi}} \langle \tau_e^i \rangle + N(\delta + 1) \left\langle \log \frac{R - a \cos \theta_j}{s_j^3} \right\rangle. \end{aligned}$$

Running through calculations analogous to those of Section 5.3.1, we finally obtain the explicit function

$$\begin{aligned} \log \mathcal{L}(a\hat{\mathbf{u}}, t_0) &= \text{const} - \frac{N}{\sigma^2} \left(\frac{1}{2} + \frac{\delta}{\pi} \right) \left(t_0^2 + \frac{n^2}{3c^2} a^2 + \frac{2n}{3cR} a^2 t_0 \right) \\ &\quad - \frac{N\delta}{\sigma} \sqrt{\frac{2}{\pi}} \left(t_0 + \frac{n}{3cR} a^2 \right) - N(\delta + 1) \frac{2}{3R^2} a^2. \end{aligned} \quad (5.40)$$

In the limit $c\sigma/R \rightarrow 0$ (that is, for a very large detector compared to the width of the scintillator response function), it can be shown that the spatial resolution at the center of a detector is given by

$$\delta a = \frac{c\sigma}{n} \sqrt{\frac{3}{\epsilon} \frac{\pi(1+\delta)}{\pi+2\delta}}. \quad (5.41)$$

Compare with the approximation $\frac{c\sigma}{n} \sqrt{\frac{3}{N}}$ for Equation (5.26). Hence, holding ϵ fixed, the resolution of an event with an average photoelectron multiplicity of $\delta = 0.5$ excess photoelectrons per PMT is a factor of $\sqrt{\pi(1+\delta)/(\pi+2\delta)}$, or 6.7%, worse than if PMTs could measure the arrival time of every photon seen. With $\delta = 1$ excess photoelectron per PMT (every hit PMT seeing an average of 2 photons), the resolution is 10.5% worse. In the limit of large δ (for instance with a high-energy event), the resolution reaches an asymptote of $\sqrt{\pi/2}$ times (about 25.3% worse) that of an ideal detector observing an event of equal energy.

Realistically, construction of an ideal detector, one that measures the time of arrival for every detected photon, would be non-trivial. One may on the other hand ask, given a detector capable of measuring time of arrival only for the first photon seen by each PMT, how the use of the statistically corrected scintillator dispersion function improves the results over the use of an uncorrected function. This comparison is equivalent to fixing N while (for the uncorrected dispersion function) setting δ to zero. In this case, the use of the corrected dispersion function is an improvement by the factor $\sqrt{\pi}/\sqrt{\pi+2\delta}$ (recall that smaller resolutions are better). For $\delta = 0.5$, the reciprocal of the improvement factor is

1.15, and for $\delta = 1$, it is 1.28; for large δ , it would theoretically improve without bound. This comparison even leaves aside the fact that for events offset from the center of the detector, use of the uncorrected scintillator dispersion function will produce a statistically biased position estimate; refer to Section 7.1 for an example.

5.5 Expected spatial distribution of reconstructed events

In this section, we leave off thinking about the magnitude of the likely error in position for a single reconstructed event, and instead consider how this error affects the spatial distribution of many events observed in a detector. We first clarify the distinction between the true and observed position distributions. If the spatial resolution of the detector were zero (infinitely good), the two would be identical. Only one distribution would need to be considered, the function $\phi(\mathbf{x})$, where the probability for an event to occur within the volume element $d^3\mathbf{x}$ of the detector would be given by $\phi(\mathbf{x}) d^3\mathbf{x}$. In the real world, however, the reconstructed position of an event will always differ somewhat from the true position. The true and observed positions of an event will henceforth be labeled \mathbf{x}_r and \mathbf{x}_d , respectively (“r” for “real” and “d” for “detected”), and the spatial distributions of the true and observed positions of events will be labeled $\phi_r(\mathbf{x})$ and $\phi_d(\mathbf{x})$, respectively.

5.5.1 Calculating the expected observed event distribution

We can define a “resolution function” of the detector $R(\mathbf{x}_r, \mathbf{x}_d) d^3\mathbf{x}_d$ to be the probability that, if the true event is at position \mathbf{x}_r , the reconstructed position of the event will be within the volume element $d^3\mathbf{x}_d$ centered about \mathbf{x}_d . More formally,

$$R(\mathbf{x}_0, \mathbf{x}_d) d^3\mathbf{x}_d \equiv P(\mathbf{x}_d \in d^3\mathbf{x}_d | \mathbf{x}_r = \mathbf{x}_0).$$

We expect that $R(\mathbf{x}_r, \mathbf{x}_d)$ can be approximated by a Gaussian in \mathbf{x}_d centered at \mathbf{x}_r :

$$R(\mathbf{x}_r, \mathbf{x}_d) = (2\pi\sigma^2)^{-3/2} e^{-\frac{(\mathbf{x}_d - \mathbf{x}_r)^2}{2\sigma^2}}. \quad (5.42)$$

The constant factor $(2\pi\sigma^2)^{-3/2}$ is needed because the integral over all space $\int R(\mathbf{x}_r, \mathbf{x}_d) d^3\mathbf{x}_d$ must be 1. The value σ is the detector's spatial resolution, which has until now been labeled δa . It is in general a function of the true event position and number of photoelectrons, $\sigma = \sigma(\mathbf{x}_r, \epsilon)$. For now we assume mono-energetic events and do not explicitly write out the energy dependence of σ .

It should be noted that this Gaussian form of the resolution function is only a simple model. It assumes (necessarily, but not sufficiently) that (1) the reconstruction is not biased, *i. e.*, has no systematic sources of error; and (2) the reconstruction error is isotropic: $\sigma_x(\mathbf{x}_r) = \sigma_y(\mathbf{x}_r) = \sigma_z(\mathbf{x}_r) = \sigma(\mathbf{x}_r)$ at each point \mathbf{x}_r in the detector. We emphasize that the model is *not* a logical consequence of the likelihood function analyses in previous sections of this chapter.

We now ask how to obtain $\phi_d(\mathbf{x})$ given $\phi_r(\mathbf{x})$. The probability that the reconstructed event will be observed within the volume element $d^3\mathbf{x}$ is given by

$$\begin{aligned}\phi_d(\mathbf{x}) d^3\mathbf{x} &= \int P(\mathbf{x} \in d^3\mathbf{x} | \mathbf{x}' \in d^3\mathbf{x}') P(\mathbf{x}' \in d^3\mathbf{x}') \\ &= \int R(\mathbf{x}', \mathbf{x}) d^3\mathbf{x} \phi_r(\mathbf{x}') d^3\mathbf{x}'\end{aligned}$$

yielding, with the insertion of equation (5.42),

$$\phi_d(\mathbf{x}) = \int \phi_r(\mathbf{x}') \frac{e^{-\frac{(\mathbf{x}-\mathbf{x}')^2}{2\sigma^2}}}{(2\pi\sigma^2)^{3/2}} d^3\mathbf{x}'. \quad (5.43)$$

The integral in \mathbf{x}' is of course taken only over the detector volume of active scintillator. (Or, equivalently, $\phi_r(\mathbf{x}')$ is defined to be zero when \mathbf{x}' is outside that volume.)

5.5.2 Radially symmetric event distributions

In order to obtain some understanding of this relationship, we for now make the simplifying assumptions that

- the detector scintillator volume and set of PMTs are spherical and centered on the origin of coordinates;
- the detector resolution is radially symmetric, and therefore is a function only of an event's distance from the origin;
- the physical distribution of events in the scintillator is also radially symmetric.

We now consider how to obtain the distribution of the reconstructed positions of events for three cases: events produced by impurities distributed homogeneously throughout the scintillator volume (“internal events”); alpha and beta particles emitted from the surface of a vessel containing the scintillator (“surface events”); and gamma rays coming into the scintillator from that surface or from outside (“external events”).

Use of radial symmetry

When the true event distribution ϕ_r is radially symmetric, the observed event distribution ϕ_d must also be radially symmetric. Without loss of generality, we may therefore work in the coordinate system in which $\mathbf{x} = |\mathbf{x}|\hat{\mathbf{z}}$, so the angle between the vectors \mathbf{x} and \mathbf{x}' is θ , the co-latitude of \mathbf{x}' . Defining $r \equiv |\mathbf{x}|$, we can expand the argument of the exponential in equation (5.43) as

$$(\mathbf{x} - \mathbf{x}')^2 = r^2 + r'^2 - 2\mathbf{x} \cdot \mathbf{x}' = r^2 + r'^2 - 2rr' \cos \theta.$$

Converting to spherical coordinates, equation (5.43) becomes

$$\begin{aligned}
\phi_d(r) &= \frac{1}{(2\pi)^{3/2}} \int d\Omega' dr' r'^2 \frac{\phi_r}{\sigma^3} e^{-\frac{r^2+r'^2}{2\sigma^2}} e^{-\frac{rr'\cos\theta'}{\sigma^2}} \\
&= \frac{2\pi}{(2\pi)^{3/2}} \int_0^R dr' r'^2 \frac{\phi_r}{\sigma^3} e^{-\frac{r^2+r'^2}{2\sigma^2}} \int_{-1}^1 d(\cos\theta') e^{-\frac{rr'\cos\theta'}{\sigma^2}} \\
&= \frac{1}{\sqrt{2\pi}} \int_0^R dr' r'^2 \frac{\phi_r}{\sigma^3} e^{-\frac{r^2+r'^2}{2\sigma^2}} \frac{2\sigma^2}{rr'} \sinh \frac{rr'}{\sigma^2} \\
&= \sqrt{\frac{2}{\pi}} \frac{1}{r} \int_0^R dr' \frac{\phi_r}{\sigma} r' e^{-\frac{r^2+r'^2}{2\sigma^2}} \sinh \frac{rr'}{\sigma^2}
\end{aligned} \tag{5.44}$$

with R defined here as the radius of the volume of active scintillator, not the distance of the PMTs from the center as in previous sections.

If ϕ_r and σ are even functions of r' (they can always be made so, since they are not physically defined for $r' < 0$ anyway), this may be simplified slightly by expanding the sinh function and taking $r' \rightarrow -r'$ in the second term:

$$\begin{aligned}
\phi_d(r) &= \frac{1}{\sqrt{2\pi} r} \int_0^R dr' \frac{\phi_r}{\sigma} r' \left[e^{-\frac{(r-r')^2}{2\sigma^2}} - e^{-\frac{(r+r')^2}{2\sigma^2}} \right] \\
&= \frac{1}{\sqrt{2\pi} r} \int_{-R}^R dr' \frac{\phi_r}{\sigma} r' e^{-\frac{(r-r')^2}{2\sigma^2}}.
\end{aligned} \tag{5.45}$$

Note the change to the bounds of integration in the final step. We always require that r itself is non-negative.

Internal event distribution function

In the case of a uniform radioactive contamination throughout the active scintillator volume V , the true distribution of internal events $\phi_r(r)$ is constant and equal to $1/V = 3/(4\pi R^3)$. Therefore, substituting into equation (5.45),

$$\phi_d(r) = \frac{3}{4\pi R^3} \frac{1}{\sqrt{2\pi} r} \int_{-R}^R dr' \frac{r'}{\sigma} e^{-\frac{(r-r')^2}{2\sigma^2}}. \tag{5.46}$$

The relevant quantity to which experimental data should be fit is not $\phi_d(r)$, but instead is the distribution function in r of reconstructed events,

$$f_d(r) = r^2 \int d\Omega \phi_d(r) = 4\pi r^2 \phi_d(r) \quad (5.47)$$

$$= \frac{3}{R^3} \frac{r}{\sqrt{2\pi}} \int_{-R}^R dr' \frac{r'}{\sigma} e^{-\frac{(r-r')^2}{2\sigma^2}}. \quad (5.48)$$

(This function, by construction, is the derivative of the function that gives the fraction of events having a reconstructed radial position less than r .)

The detector resolution σ may be determined experimentally in a number of different ways, or estimated as in Section 5.3.4. The functions $\phi_d(r)$ and $f_d(r)$ are plotted in Figure 5.4 for a volume of scintillator with a radius of 1 meter, assuming a constant value of σ for the three cases $\sigma = 10, 15,$ and 20 cm. These are comparable to the values for Borexino's Counting Test Facility.

Event distribution functions for surface α particles and electrons

Since the average scintillator penetration length of α particles in an organic scintillator such as pseudocumene is < 1 mm, and that of 1 MeV electrons is ~ 1 cm, the travel distances of these particles originating from the scintillator containment vessel are negligible compared to σ . Then ϕ_r may be approximated by the delta function

$$\phi_r(r) = \frac{\delta(r - R + \epsilon)}{4\pi R^2} \quad (5.49)$$

(where we let $\epsilon \rightarrow 0$ after any integration).

Substituting this into equation (5.44), the reconstructed event density and radial position become

$$\phi_d(r) = \sqrt{\frac{2}{\pi}} \frac{e^{-\frac{R^2}{2\sigma^2}}}{4\pi R} \frac{e^{-\frac{r^2}{2\sigma^2}}}{\sigma r} \sinh \frac{r R}{\sigma^2} \quad (5.50)$$

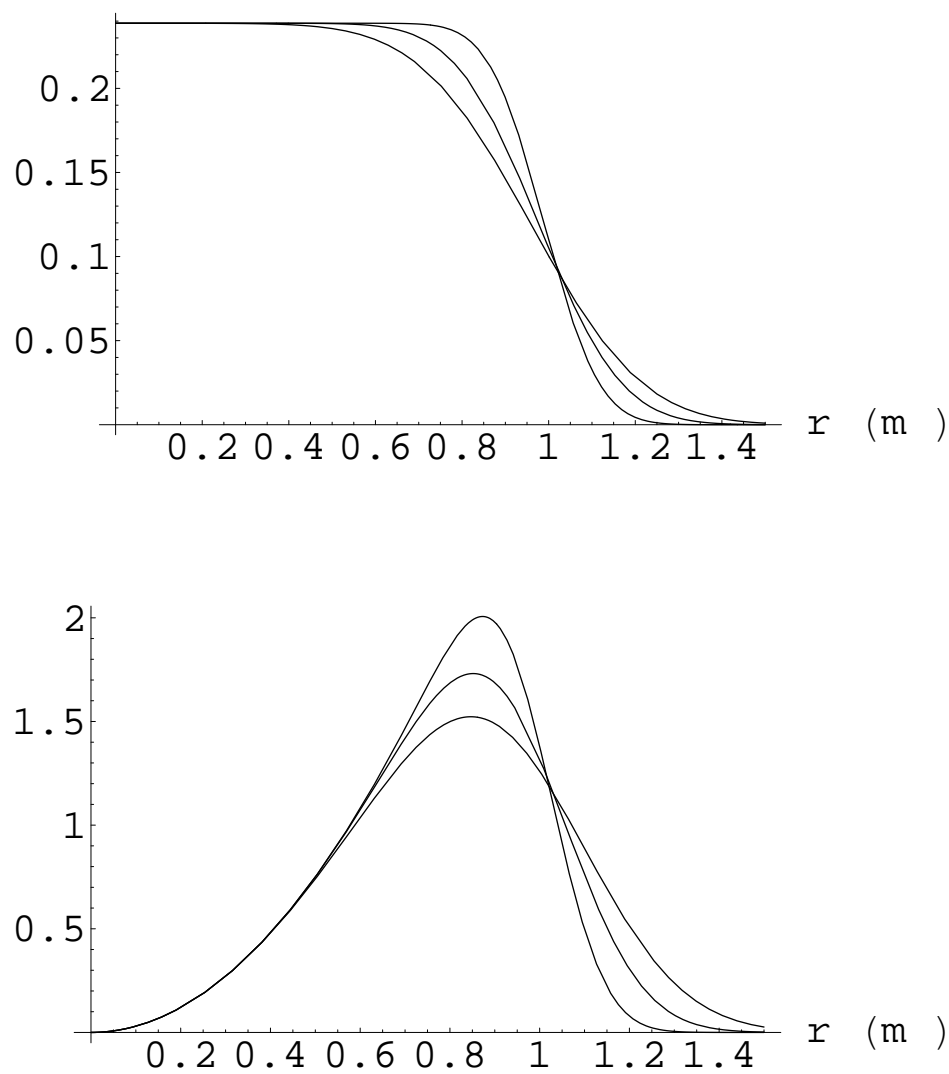


Figure 5.4: Internal distribution functions $\phi_d(r)$, top, and observed event radial distribution functions $f_d(r)$, bottom, for constant $\sigma = 10, 15$ and 20 cm.

$$f_d(r) = \sqrt{\frac{2}{\pi}} \frac{r}{R} \frac{e^{-\frac{R^2+r^2}{2\sigma^2}}}{\sigma} \sinh \frac{rR}{\sigma^2} = \frac{1}{\sqrt{2\pi}} \frac{r}{\sigma} \frac{1}{R} \left[e^{-\frac{(r-R)^2}{2\sigma^2}} - e^{-\frac{(r+R)^2}{2\sigma^2}} \right] \quad (5.51)$$

where σ is the value of $\sigma(r)$ evaluated at $r = R$. These functions are graphed for various values of $\sigma(R)$ in Figure 5.5.

Event distribution functions for external γ rays

Gamma rays, unlike α and β particles, can travel tens of centimeters in a liquid scintillator before being completely absorbed. A Monte Carlo simulation would be necessary to evaluate their true event position distribution accurately, but a crude estimation can be made analytically by assuming that all the energy of each γ ray is absorbed at once (no scattering). The results of a Monte Carlo simulation will be examined in Section 9.4.

Let the average scintillator penetration length of a γ ray of specific energy be λ , and assume $\lambda \ll R$, the radius of the scintillator volume. If s is the total distance traveled by an emitted particle, the distribution of s is of course given by

$$g(s) ds = (1/\lambda)e^{-s/\lambda} ds. \quad (5.52)$$

We first calculate the true distribution $\phi_r(r)$ of events produced by absorption of γ rays originating on the scintillator containment vessel. Consider the geometry shown in Figure 5.6, in which a γ ray produced at point A penetrates a distance s into the volume of scintillator before being absorbed at point B. The angle ψ is that between the γ ray path and a normal vector into the scintillator. The Law of Cosines gives us $r^2 = R^2 + s^2 - 2Rs \cos \psi$. The question is then, what is the distribution function $f_r(r)$ for the distance from the center at which a γ ray originating on the vessel is absorbed?

We know that $\cos \psi$ is a uniformly distributed random variable on the interval $(0, 1]$ (recall that a value of $\cos \psi \leq 0$ would imply an event outside the scintillator, which cannot be detected). Hence, for a fixed value of s , r^2 is a uniform random variable on $[(R-s)^2, R^2 + s^2]$.

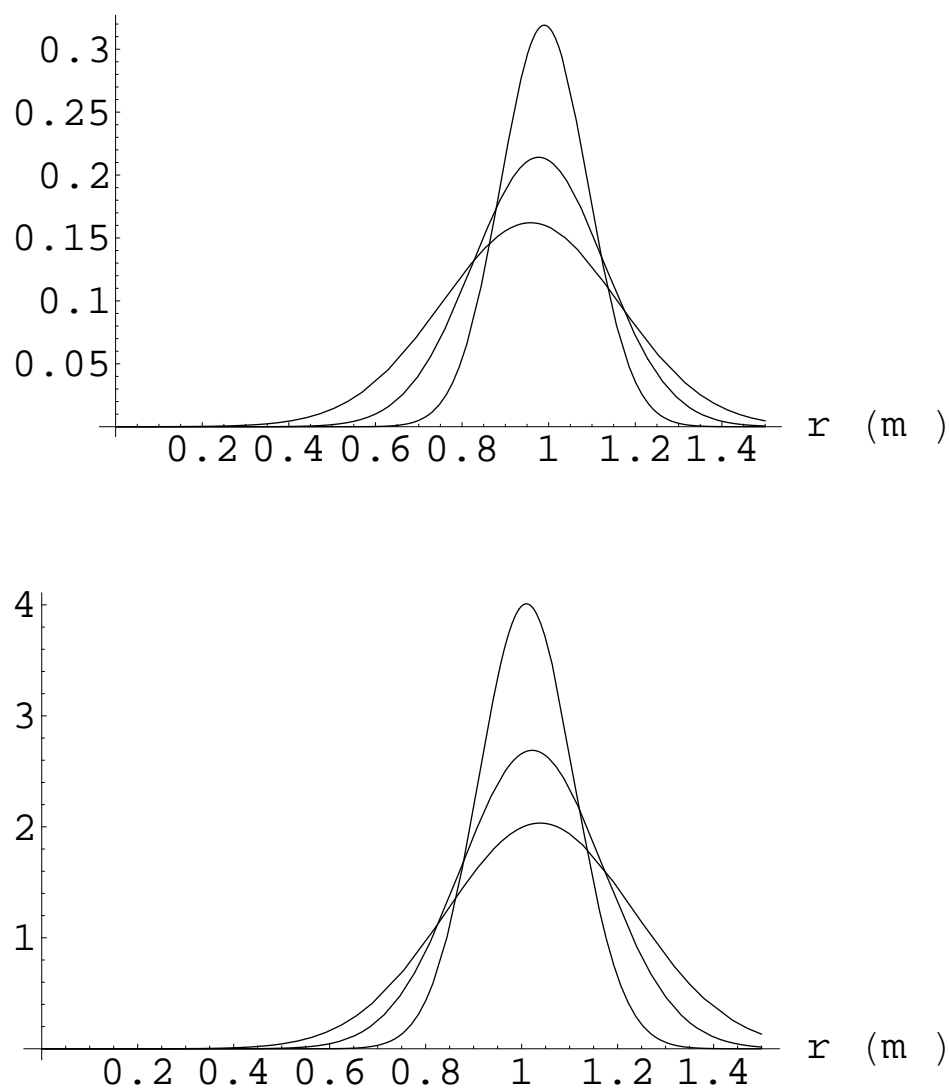


Figure 5.5: Surface distribution functions $\phi_d(r)$, top, and observed surface event radial distribution functions $f_d(r)$, bottom, for $\sigma = 10, 15$ and 20 cm.

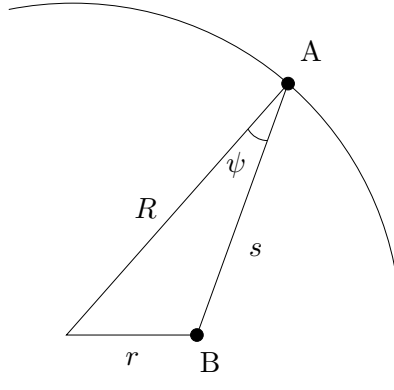


Figure 5.6: Geometry of surface event distribution calculation.

The change of variables theorem for a random variable tells us that therefore r (for a fixed value s) has the distribution

$$P(r \in dr | s \in ds) = \begin{cases} r dr / 2Rs, & |R - s| \leq r < \sqrt{R^2 + s^2} \\ 0 & \text{otherwise.} \end{cases} \quad (5.53)$$

(The factor of $1/2$ comes about because we reject the non-physical case $r < 0$.)

If it is assumed that $0 \leq r < R$, then the above function is non-zero only when $R - r \leq s \leq R + r$. Therefore the distribution of r without the constraint of fixed s becomes

$$\begin{aligned} P(r \in dr) \equiv f_r(r) dr &= \int_{s=R-r}^{R+r} P(r \in dr | s \in ds) P(s \in ds) \\ &= \int_{s=R-r}^{R+r} \frac{r dr}{2Rs} \frac{e^{-s/\lambda}}{\lambda} ds \\ &= \frac{r dr}{2R\lambda} \left[\text{ei} \left(-\frac{R+r}{\lambda} \right) - \text{ei} \left(\frac{r-R}{\lambda} \right) \right] \end{aligned} \quad (5.54)$$

where ei is the exponential integral function $\text{ei}(x) \equiv -\int_{-x}^{\infty} (e^{-t}/t) dt$. Therefore, in the case of a uniform distribution of γ rays produced at the scintillator containment vessel, we obtain

$$\phi_r(r) = \frac{f_r(r)}{4\pi r^2} = \frac{1}{8\pi Rr\lambda} \Theta(R-r) \left[\text{ei} \left(-\frac{R+r}{\lambda} \right) - \text{ei} \left(\frac{r-R}{\lambda} \right) \right] \quad (5.55)$$

($\Theta(x)$ being the Heaviside function: one for $x > 0$, zero otherwise).

As an aside, note that the previous two equations are not properly normalized. Their respective integrals over the volume of the vessel and over the range $0 \leq r < R$ do not evaluate to 1, but instead to the value

$$\int_V \phi_r(r) dV = \int_0^R f_r(r) dr = \frac{1}{2} \left[1 - \frac{\lambda}{2R} \left(1 - e^{-2R/\lambda} \right) \right]. \quad (5.56)$$

This should not come as a surprise. The quantity above represents the fraction of γ rays emitted from the containment vessel surface that are actually absorbed within the scintillator. The factor of $\frac{1}{2}$ in front represents the fact that a γ ray produced at the surface has only a 50% chance of being directed inward instead of outward. As the ratio λ/R increases, the chance for a random γ ray to be absorbed within the scintillator becomes ever smaller.

The true event distributions $\phi_r(r)$ and the observed radial distribution functions $f_d(r)$ for varying values of λ are plotted in Figure 5.7. The latter is of course obtained from the former by substituting into Equation (5.44) and multiplying by $4\pi r^2$:

$$f_d(r) = \frac{1}{\sqrt{2\pi}} \frac{r}{R\lambda} \int_0^R dr' \left[\text{ei} \left(-\frac{R+r'}{\lambda} \right) - \text{ei} \left(\frac{r'-R}{\lambda} \right) \right] \frac{1}{\sigma} e^{-\frac{r^2+r'^2}{2\sigma^2}} \sinh \frac{rr'}{\sigma^2}. \quad (5.57)$$

In fact, most γ rays will originate outside the scintillator containment vessel, for instance from the PMTs. The event distribution at a fixed radius r within the scintillator for a fixed energy will then be the integral of Equation (5.55) over all external sources:

$$\phi_r(r) = \frac{1}{8\pi r \lambda} \int_R^\infty \rho(r') \frac{dr'}{r'} \Theta(r' - r) \left[\text{ei} \left(-\frac{r+r'}{\lambda} \right) - \text{ei} \left(\frac{r-r'}{\lambda} \right) \right] \quad (5.58)$$

where $\rho(r')$ is the normalized density of γ ray emissions at the given energy within the spherical shell of radius r' . This formula assumes spherical symmetry. As before, this function may be substituted into equation (5.44) and multiplied by $4\pi r^2$ to obtain the observed event distribution in r , $f_d(r)$.

It must be noted again that this derivation is not completely realistic. A better model of external γ ray behavior will be considered in Section 9.4.1.

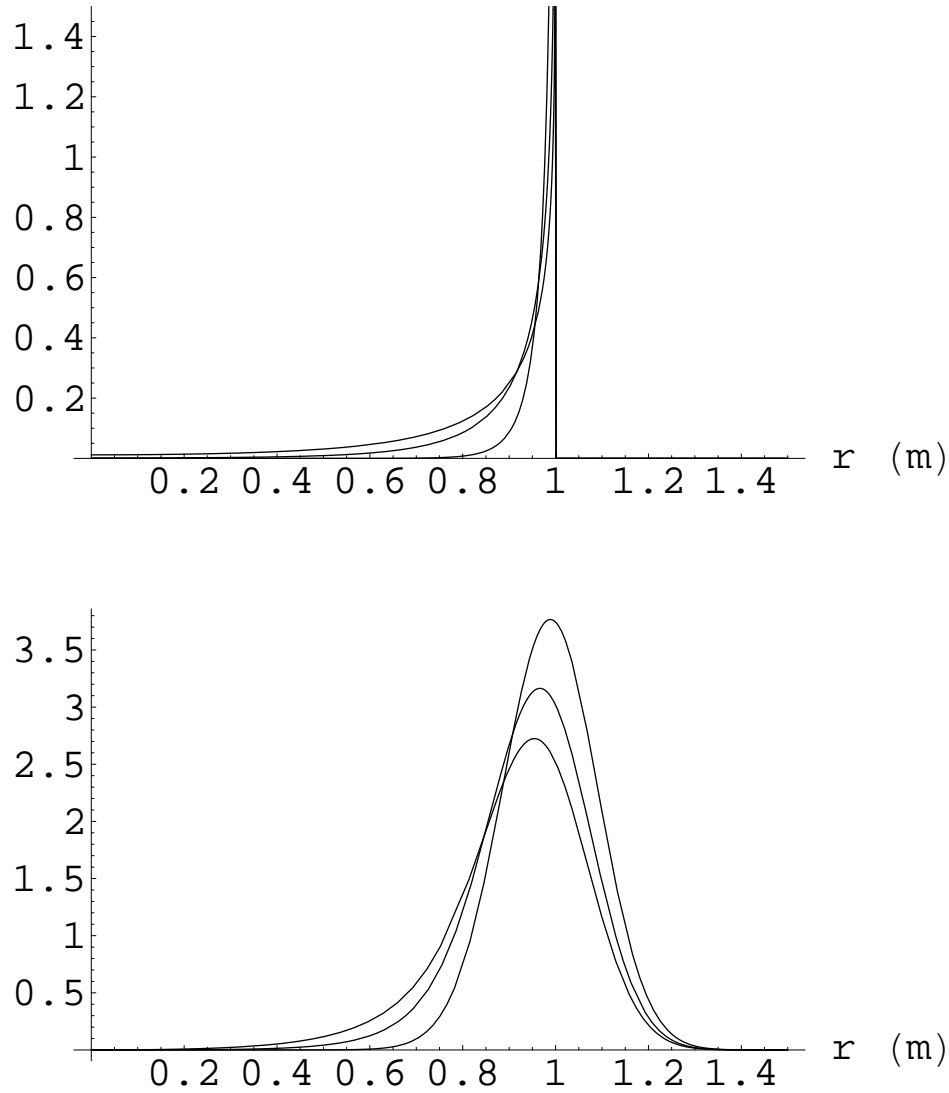


Figure 5.7: True distribution functions $\phi_r(r)$, top, and observed radial distribution functions $f_d(r)$, bottom, for γ rays with mean scattering distances of $\lambda = 5, 15$ and 25 cm, and (in the second plot) constant detector resolution $\sigma = 10$ cm. The vertical asymptotes at $r = 1$ m in the upper graph result from the non-physical assumption that the vessel film thickness is infinitesimal yet emits γ rays at a finite rate. In these graphs, the factor of $\frac{1}{2}$ resulting from Equation (5.53) has been suppressed.

5.5.3 Previously used radial distribution functions

Above, we have followed the steps of assuming a true spatial distribution of events $\phi_r(r)$, deriving from this function the observed spatial distribution $\phi_d(r)$, and multiplying by $4\pi r^2$ to obtain a reconstructed radial distribution function:

$$\phi_r(r) \xrightarrow[3\text{-D Gaussian}]{\text{convolve with}} \phi_d(r) \xrightarrow{\times 4\pi r^2} f_d(r). \quad (5.59)$$

The radial distribution functions $f_d^*(r)$ used in previous CTF analysis work resulted from the assumption that the true radial distribution of events $f_r(r) \equiv 4\pi r^2 \phi_r(r)$ can be convolved with a one-dimensional Gaussian, $e^{-\frac{(r-r')^2}{2\sigma^2}}/\sqrt{2\pi}\sigma$, to produce the radial distribution of reconstructed events. That is,

$$\phi_r(r) \xrightarrow{\times 4\pi r^2} f_r(r) \xrightarrow[1\text{-D Gaussian}]{\text{convolve with}} f_d^*(r). \quad (5.60)$$

For a particular event distribution $\phi_r(r)$, the function $f_d^*(r)$ is not necessarily equal to the function $f_d(r)$ defined in equation (5.47).

Given a constant internal distribution function $\phi_r = 1/V = 3/(4\pi R^3)$, the true radial event distribution is

$$f_r(r) = 4\pi r^2 \phi_r = \frac{3r^2}{R^3}. \quad (5.61)$$

The convolution (assuming constant σ) yields

$$f_d^*(r) = \frac{k_b}{\sqrt{2\pi}\sigma} \int_0^R f_r(r') e^{-\frac{(r-r')^2}{2\sigma^2}} dr' \quad (5.62)$$

$$= \frac{3}{R^3} \frac{k_b}{\sqrt{2\pi}\sigma} \int_0^R dr' r'^2 e^{-\frac{(r-r')^2}{2\sigma^2}}, \quad (5.63)$$

with k_b a normalization constant chosen such that $\int_0^\infty f_d^*(r) dr = 1$. Specifically,

$$k_b = \left[\frac{1}{2} \left(1 + \operatorname{erf} \frac{R}{\sqrt{2}\sigma} \right) + \frac{1}{\sqrt{2\pi}} \frac{\sigma}{R} e^{-\frac{R^2}{2\sigma^2}} - \sqrt{\frac{2}{\pi}} \left(\frac{\sigma}{R} \right)^3 \left(1 - e^{-\frac{R^2}{2\sigma^2}} \right) \right]^{-1}. \quad (5.64)$$

In the limit $\sigma/R \ll 1$, we find $k_b \rightarrow 1$. (With $R = 1$ m and $\sigma = 15$ cm, approximating k_b as 1 is already accurate to within 0.3 percent. In the CTF 3, σ is more on the order of 10 to 12 cm.)

We now consider the surface event distribution. Using the spatial distribution of equation (5.49), we obtain $f_r(r) = r^2 \delta(r - R + \epsilon)/R^2$, and the convolution with a Gaussian in r results in

$$f_d^*(r) = \frac{k_s}{\sqrt{2\pi} \sigma R^2} \int_0^R dr' r'^2 \delta(r' - R + \epsilon) e^{-\frac{(r-r')^2}{2\sigma^2}} = \frac{k_s}{\sqrt{2\pi} \sigma} e^{-\frac{(r-R)^2}{2\sigma^2}} \quad (5.65)$$

(taking $\epsilon \rightarrow 0$ in the last step) with the normalization requiring

$$k_s = 2 \left(1 + \operatorname{erf} \frac{R}{\sqrt{2} \sigma} \right)^{-1}. \quad (5.66)$$

In the limit $\sigma/R \ll 1$, we have $k_s \rightarrow 1$ with an error of < 0.1 ppb at $\sigma = 16$ cm.

Figure 5.8 shows a comparison of the reconstructed radial distribution functions developed in equations (5.48) and (5.51) with the functions previously used in CTF analysis [equations (5.63) and (5.65)], using the limiting values of $k_b = k_s = 1$. Notable differences are that

- the previously used functions do not quite go to zero at $r = 0$;
- the previously used functions have peaks at smaller values of r than the corresponding functions developed above.

It is not simple to determine how the use of these functions instead of the “correct” ones discussed earlier in this section would affect analyses of internal and surface events in the CTF. The differences between the two sets of functions presumably permit the “correct” ones to fit the observed data slightly better. Still, the two sets of functions are not really that different. In addition, other effects such as the radial dependence of σ and the presence of γ events from external sources would tend to obscure the differences, so their effects upon real experimental analyses should be small.

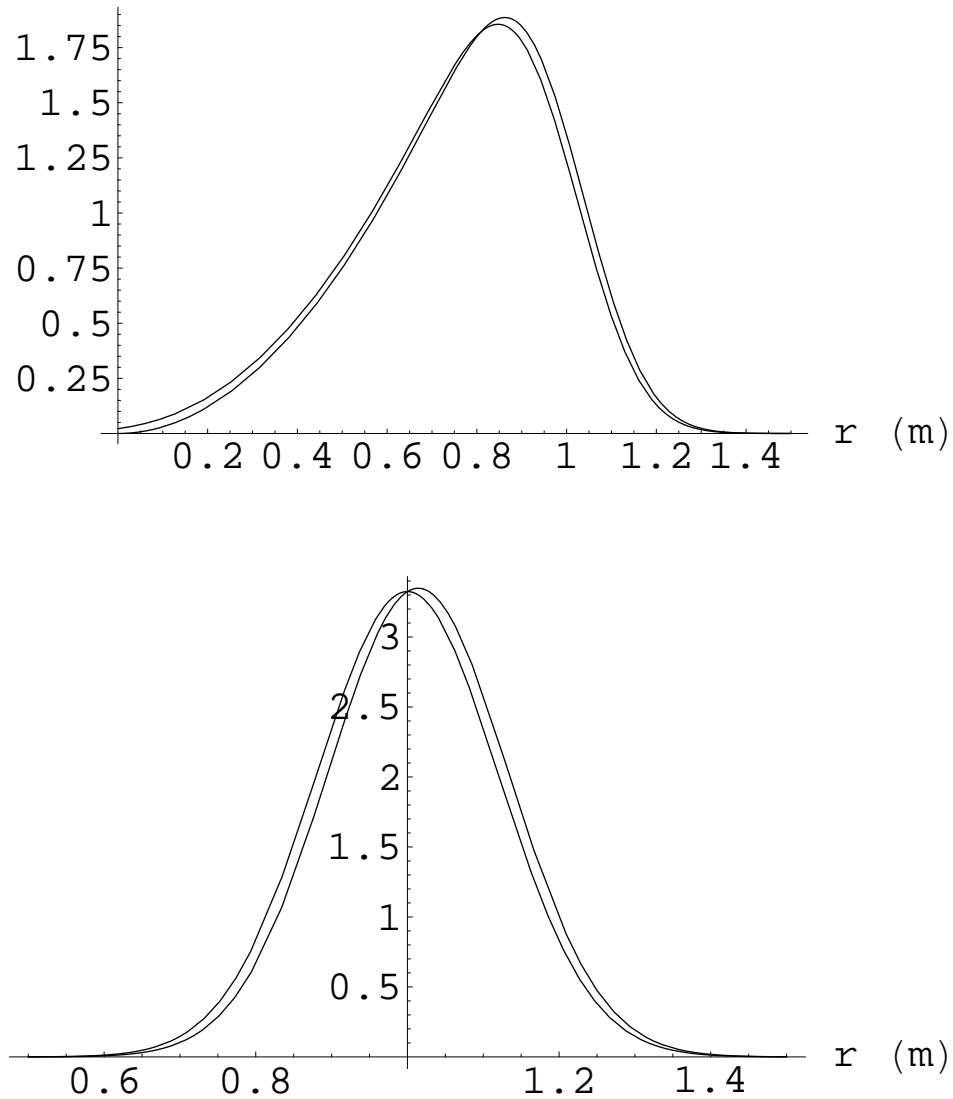


Figure 5.8: Comparison of the above-developed internal (top) and surface (bottom) radial distribution functions, $f_d(r)$, with those previously used in CTF analysis, $f_d^*(r)$, assuming $\sigma = 12$ cm and setting $k_b = k_s = 1$. The previously used functions are those with peaks at smaller values of r .

5.5.4 Cylindrical geometries

Until now this chapter has considered event distributions in a spherically symmetric detector. Consider, though, the problem of a spherical detector which has two “hot spots” on opposite sides; call these the north and south poles. Suppose we want to make a fit of the observed radial distribution of events to a weighted sum of the internal, surface, and external distribution functions $f_d(r)$ defined above. A naïve treatment using these functions, ignoring the θ and ϕ coordinates of events, will yield overly pessimistic conclusions about the average number of surface events per unit area, and the internal and external event distributions may be swamped by the hot spots. Instead, the hot spots should somehow be excluded from the data. This can be done in two obvious ways:

- Cut out wedges (cones) around the poles. Doing so will exclude equal ratios of scintillator containment vessel surface and scintillator fluid volume from the analysis.
- Consider only a relatively thin slice through the equator of the scintillator containment vessel, and analyze it assuming a cylindrical geometry.

The latter solution requires us to develop a new set of reconstructed event distributions for a cylindrical geometry. These may also be useful in other circumstances, since most particle detectors at beam colliders are cylindrical as well.

Without loss of generality, aside from the assumptions pointed out in Section 5.5.1, we may start again with Equation (5.43):

$$\phi_d(\mathbf{x}) = \int \phi_r(\mathbf{x}') \frac{e^{-\frac{(\mathbf{x}-\mathbf{x}')^2}{2\sigma^2}}}{(2\pi\sigma^2)^{3/2}} d^3\mathbf{x}'.$$

If we assume that the cylinder is infinitely long, or at least of length $L \gg \sigma$; and that the true event distributions are not z -dependent (the z -axis being the axis of the cylinder); then the problem is essentially two-dimensional due to its translational invariance. The above

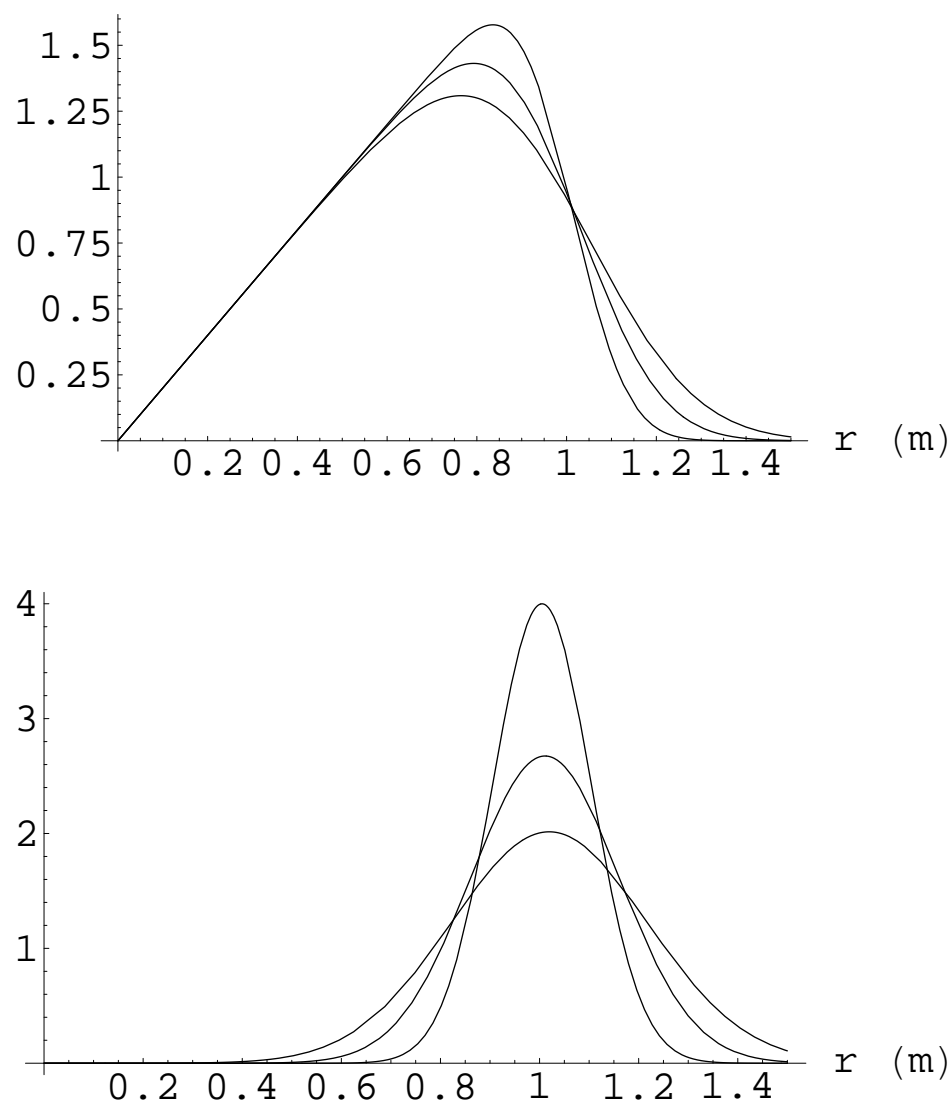


Figure 5.9: Internal and surface radial event distributions, $f_a(r)$, for a cylindrical geometry detector. They are shown for constant values of σ at 10, 15, and 20 cm.

equation may be converted into cylindrical coordinates and rewritten as

$$\phi_d(r, \theta) = \frac{1}{(2\pi)^{3/2}} \int d\theta' dz' dr' r' \frac{\phi_r}{\sigma^3} e^{-\frac{(\mathbf{x}-\mathbf{x}')^2}{2\sigma^2}}. \quad (5.67)$$

(Note that r is now the coordinate perpendicular to the z axis, not the spherical radial coordinate.)

With true event distributions that are also rotationally invariant around the z axis (no θ dependence), we may perform the integration in a primed coordinate system specified such that $\theta = 0$ and $z = 0$. That is,

$$(\mathbf{x} - \mathbf{x}')^2 = r^2 + r'^2 + z'^2 - 2\mathbf{x} \cdot \mathbf{x}' = r^2 + r'^2 + z'^2 - 2rr' \cos \theta'. \quad (5.68)$$

Conveniently, the integral in z' simply evaluates to $\sqrt{2\pi\sigma^2}$, leaving

$$\begin{aligned} \phi_d(r) &= \frac{1}{2\pi} \int_0^R dr' r' \frac{\phi_r}{\sigma^2} e^{-\frac{r^2+r'^2}{2\sigma^2}} \int_0^{2\pi} d\theta' e^{\frac{rr'}{\sigma^2} \cos \theta'} \\ &= \int_0^R dr' r' \frac{\phi_r}{\sigma^2} I_0\left(\frac{rr'}{\sigma^2}\right) e^{-\frac{r^2+r'^2}{2\sigma^2}}, \end{aligned} \quad (5.69)$$

where $I_0(x)$ is the zeroth-order modified Bessel function of the first kind.

Using $dV = r dr dz d\theta \rightarrow 2\pi r dr \Delta z$, and the respective true internal and surface distributions $1/(\pi R^2 \Delta z)$ and $\delta(r - R + \epsilon)/(2\pi R \Delta z)$, we immediately have the reconstructed distributions of internal and surface events,

$$f_d(r) \text{ [internal]} = \frac{2r}{R^2} \int_0^R dr' \frac{r'}{\sigma^2} I_0\left(\frac{rr'}{\sigma^2}\right) e^{-\frac{r^2+r'^2}{2\sigma^2}} \quad (5.70)$$

$$f_d(r) \text{ [surface]} = \frac{r}{\sigma^2} I_0\left(\frac{rR}{\sigma^2}\right) e^{-\frac{r^2+R^2}{2\sigma^2}}. \quad (5.71)$$

The ϕ_d functions look very similar to those for spherical geometries. The radial distribution functions $f_d(r)$ are shown in Figure 5.9. Notice how the internal reconstructed distribution function obeys $f_d(r) \sim r$ for small r , as opposed to the spherical internal distribution function that goes like r^2 .

Although largely irrelevant to a thin slice through a spherical detector, but perhaps useful in (*e. g.*) a wire drift chamber, it is not hard to show that the assumption of complete isotropy in σ is overkill in the geometry of an infinitely long cylinder. It is sufficient to have $\sigma_x = \sigma_y$, with a different value for σ_z , without affecting the results above; one would start from this modified form of Equation (5.42):

$$R(\mathbf{x}_r, \mathbf{x}_d) = \frac{1}{2\pi\sigma_{\perp}^2} e^{-\frac{(\mathbf{x}_d - \mathbf{x}_r)_{\perp}^2}{2\sigma_{\perp}^2}} \frac{1}{\sqrt{2\pi\sigma_z^2}} e^{-\frac{(z_d - z_r)^2}{2\sigma_z^2}}. \quad (5.72)$$